Coaxial 4D printing of vein-inspired thermoresponsive channel hydrogel actuators

Daria Podstawczyk, Martyna Nizioł, Piotr Śledzik, Julia Simińska-Stanny, Anna Dawiec-Liśniewska, Amin Shavandi*

D. Podstawczyk, P. Śledzik, M. Nizioł, J. Simińska-Stanny
Department of Process Engineering and Technology of Polymer and Carbon Materials, Faculty of Chemistry, Wroclaw University of Science and Technology, Norwida 4/6, 50-373 Wroclaw, Poland
E-mail: daria.podstawczyk@pwr.edu.pl, ORCID ID: 0000-0003-0950-6836

A. Dawiec-Liśniewska
Department of Advanced Materials Technologies, Faculty of Chemistry, Wroclaw University of Science and Technology, Smoluchowskiego 25, 50-372 Wroclaw, Poland

J. Simińska-Stanny, A. Shavandi
BioMatter unit - École Polytechnique de Bruxelles, Université Libre de Bruxelles (ULB), Avenue F.D. Roosevelt, 50 - CP 165/61, 1050 Brussels, Belgium.

Keywords: additive manufacturing, perfusion, stimulus-responsive polymers, coaxial extrusion, functional inks, direct ink writing

Abstract

Although significant progress has been made in coaxial printing of vascularized tissue models, this technique has not yet been used to fabricate stimulus-responsive scaffolds capable of shape change over time. Here, we propose a new method of direct ink printing with a coaxial nozzle, coaxial 4D printing, enabling the manufacturing of thermoresponsive constructs embedded with a network of interconnected channels. In our approach, a poly(N-isopropylacrylamide) (PNIPAAm)-based thermoink is coaxially extruded into either core/sheath microfibers or microtubes. PNIPAAm renders a hydrogel temperature-sensitive and endows it with a shape-morphing property both at the micro- and macroscale. Specifically, the lumen diameter of the microtubes can be controlled by temperature by 30%. The macrostructural soft actuators can undergo programmed and reversible temperature-dependent shape changes due to the structural anisotropy of the hydrogel. The permeability tests

demonstrate that the hydrogel can possess enough strength to maintain the hollow channels without breaking. *In vitro* tests confirm the biocompatibility of our material with EA.hy926 cells, paving the avenue for new perfusable soft robots, active implants, or vascularized tissue models. Finally, we combined microalgae *Chlamydomonas reinhardtii* with our hydrogels to fabricate materials having functions of both living microorganisms and stimuli-responsive polymers towards creating engineered living materials (ELMs) with a vein-like geometry.

1. Introduction

Nowadays, due to the growing demand for smart materials that can change shape or functionality in response to external stimuli in a controllable way, soft robotics is one of the most rapidly growing fields attracting scientists specializing in mechanical and biomedical engineering. Bioinspired soft robots are designed to mimic biological systems and create adaptable and flexible interactions with complex objects and surroundings.[1] Biomedical and tissue engineering applications of such systems require materials that are concomitantly biocompatible and capable of altering their chemical, physical, and/or mechanical properties upon exposure to external triggers. Stimuli-responsive hydrogels are excellent candidates for soft biorobotics with their biodegradability and cytocompatibility,[2] high water content, and unique ability to respond to a variety of triggers including electric[3] and magnetic[4,5] fields, light,[6,7] temperature,[8] or ionic strength.[9] Those hydrogel systems usually exhibit layered, patterned, or oriented internal structures providing them with anisotropy and consequently shape-morphing properties. However, most bioinspired hydrogel-based robots have simplified geometry (e.g. bilayer) lacking the circulatory systems found in living organisms, and hence are unable to reproduce their efficiency and autonomy.[10] Some elastomeric soft robots use patterns of non-random embedded pneumatic or hydraulic networks of hollow fibers for activation.[11] Only one study reports a hydrogel-based system with randomly interconnected microchannels that improve actuation in soft robotic gripping devices.[12] So far, hydrogels with a vein-like network have been used in non-robotic applications to imitate hollow vascular analogs and help transport water and nutrients to support immobilized cells.[13]

Recently, various techniques have been used to ~~integrate~~ introduce microchannels into hydrogels for various biomedical and tissue engineering applications, including sacrificial writing into functional tissue[14] or directional freeze-drying.[15] Among them, coaxial 3D printing has arguably captured the most attention on account of the easy and inexpensive manufacturing of complex multimaterial structures in a one-step fabrication. Coaxial 3D printing (Coax3DP) is a microextrusion printing technique that enables the simultaneous

extrusion of multiple materials through coaxial nozzles to create microstructures with different geometries from microtubes,[16,17] through Janus microwires[18] to core-shell fibers[19]. Most applications of the Coax3DP have been reported in biomedicine, especially in vascular tissue engineering,[17,20] articular cartilage,[21] bone tissue,[22,23] and cancer model creation.[24,25] Coaxial printing seems to be an excellent technique that enables cells to be directly encapsulated and cultured within the three-dimensional (3D) hydrogel matrix of the perfusable microtubes/microfiber or seeded onto their surfaces to mimic functional tissues.[26] For example, a one-step strategy using a microfluidic coextrusion device was proposed to produce mature functional blood vessels.[27] A hollow alginate hydrogel tube was covered by an extracellular matrix which directed the self-assembly of both endothelial cells (ECs) and smooth muscle cells leading to the formation of fully active "vessoloids". In another approach, the coaxial 3D cell-printing technique was used to fabricate hollow tubes mimicking the vascular parenchyma of native kidney tissue.[28] *In vivo* tests confirmed that a long-term graft could integrate with the animal's existing kidney tissue and help restore normal kidney function. However, despite numerous fascinating studies on 3D coaxial bioprinting of cell-containing materials,[29–31] there are no reports on the research and development of 3D coaxially printed fibers and tubes with entrapped live microorganisms such as bacteria, fungi, or microalgae to create a new generation of engineered living materials (ELMs).[32]

Another considerable progress in the 3D printing field that can have significant implications for biomedical and material engineering is 4D printing (4DP).[33] 4DP enables a 3D printed structure to self-transform in shape and functions upon exposure to external triggers, such as light,[34] heat,[35,36] magnetic[37] or electrical field,[3] and pH[38] over time.[39] Recently, time as the 4th dimension has also been merged with 3D bioprinting leading to 4D bioprinting (4DBP).[34] In 4DBP, stimuli-responsive 4D-printed multi-material structures can mimic the native tissue anisotropic microenvironment better than single-material 3D-printed constructs by providing heterogeneous architecture with programmable dynamic responses to external stimuli.[33] One of the most outstanding applications of 4D bioprinting is the creation of mature functional perfusable tissue models capable of changing their functionality in time.[40–42] It is, therefore, simply a matter of time until 4D bioprinting is integrated with a coaxial nozzle for 4D vascularized tissue fabrication. A great foundation for this approach has been proposed only recently by Wang et al. who presented a versatile microfluidic 3D printing strategy to fabricate black phosphorus-incorporated PNIPAAm-based scaffolds with photothermal responsive channels for improving vascularization and bone regeneration.[34] Multichannel scaffolds exhibited reversible swelling and shrinkage features during NIR

irradiation. Moreover, photothermal responsive channels with embedded BP nanosheets promoted pre-vascularization and *in situ* biomineralization by improving endothelial cell proliferation and osteogenic differentiation. In another study, Zhang et al. fabricated, using 3D printing with in-house coaxial needles, core-shell (poly (N-isopropylacrylamide-co-acrylic acid (p(NIPAAm-AA)- fibrin) fibers embedded with endothelial cells (HUVECs) to mimic the physiological organization of skin tissue. Multilayered artificial skin structure exhibited cornification of the epidermis layer and sprouting of the subcutaneous HUVECs cells after air-liquid introduction for 2 weeks.[43]

However, as of our current investigations, coaxial 4D direct printing has not been used for the fabrication of (1) live microorganisms-containing materials or (2) thermo-responsive or perfusable microtubular soft actuators and robots and (3) their combination, despite numerous successful applications of uniaxial 4DP and 4DBP in the fabrication of multimaterial and multifunctional objects and tissue models. To fill these gaps, we propose a vein-inspired design of thermoresponsive hydrogel scaffolds with a network of perfusable channels and the ability to change shape in response to temperature. In our previous work, we developed several poly(N-isopropylacrylamide) (PNIPAAm)-based thermoinks with high printability and excellent properties of temperature-dependent shape-morphing behavior. [36] Among them, the thermoink with the most promising features (the highest thermal response and satisfactory printability) was selected for this study. The combination of alginate with the stimuli-responsive property and the coaxial 3D direct printing leads to the development of a new manufacturing strategy, one-step coaxial 4D direct ink printing (Coax4DIP). As shown by Li et al., photocuring combined with ionic crosslinking strengthens the final structure after printing.[44] Here, the interpenetrating network (IPN) of covalently and ionically crosslinked hydrogels was designed to maintain the structural integrity of the hydrogel network, without compromising the printing quality.

We demonstrate that the thermoink can be coaxially coextruded with other materials to produce hydrogel microtubes. A channel-embedded hydrogel is fabricated by shaping the microtubes into a sheet actuator with a designed geometry and the capability of thermal actuation. We show that the diameter of the microtube can be tuned dually by changing the nozzle size and through temperature-dependent swelling/deswelling of the hydrogel. The tube microstructure exhibits radial and longitudinal network and pore alignment, and, consequently, it swells or shrinks anisotropically. These phenomena drive out-of-plane deformation of the macrostructure (channel hydrogel actuator, Coax4Dgel), leading to its self-rolling or bending motion at temperatures near the lower critical solution temperature (LCST) of the hydrogel.

The channel structure improves this process by increasing the rate of the hydrogel's hydration from the inside. We believe that our channel thermoresponsive actuator paves a new avenue for the fabrication of perfusable soft biorobots or engineered muscle tissue. We next show that both the microtubes and channel structures are permeable and support the endothelial cell growth towards the advanced vascular systems with controllable vein size and perfusion. Finally, Coax4DIP was used to manufacture mutlimaterial microtubular constructs with microalgal cells immobilized either in the core or shell. The microorganisms were evenly distributed within the hydrogel and did not tend to escape to the surrounding medium when cultured for 7 days. We, therefore, believe that our method provides a versatile tool to produce the next generation of sophisticated photosynthetic engineered living materials which in their capacity as a novel immobilization technique not only can prevent cells from leakage, but also create responsive, patterned constructs in a one-step process.

2. Results and discussion

2.1. Coaxial 4D printing procedure

Although coaxial 3D printing of vasculature-mimicking systems ~~has been~~ has been known for some time now,[26,31,32] its application to print stimuli-responsive materials has never been investigated. So far core-sheath structures comprising PNIPAM and alginate have been reported as highly potent in atmospheric water harvesting, significantly increasing the water capture ratio.[45] However, these constructs were not fabricated in single-step coaxial printing, but in multimodal assembling steps, mainly involving molding. In the strategy proposed by Wang et al.,[34] the standard 3D printer nozzle was replaced with custom-made capillary microfluidic chips, not a typical coaxial nozzle. Although it enabled the fabrication of reproducible thermosensitive channel hydrogels capable of controlling their shrinkage/swelling upon exposure to near-infrared irradiation, the customization of the nozzle may make the whole process more difficult to repeat. The scaffolds provided a platform for modulating cellular behavior, specifically promoting cellular infiltration into the scaffold channels. Thermally-induced deformation of scaffolds and diameter change of channels have not been investigated. In contrast, ~~This~~ our study explores ~~the coaxial~~ 4D printing using a standard coaxial nozzle of thermosensitive materials to fabricate microtubes and channel scaffolds capable of size and shape change in response to temperature. In our previous work, we introduced a shear-thinning ink composed of laponite XLG (LAP), and an interpenetrating network of PNIPAAm and alginate (ALG) for 4D printing of thermoresponsive soft actuators.[36] Here, we used a slightly modified thermoink to propose and investigate the direct ink writing (DIW) technique of shape-morphing materials operating on a microfluidic nozzle,

which we called coaxial 4D direct ink printing. **Figure 1a** demonstrates the Coax4DIP concept. First, the precursor of the shape-memory hydrogel (ink) was formulated. Printable composite thermoink was made by mixing the aqueous solution of N-isopropylacrylamide (NIPAAm), N,N'-methylenebis(acrylamide) (MBA), and Irgacure 2959 (I2959) in a molar ratio of 10:0.6:0.5 with ALG and LAP with a mass ratio of 1:6. Next, the geometry and pattern were designed to mimic nature-inspired systems, systems, e.g. vessel networks.[46] We reproduced the 3D hydrogel discs (5 layers, a diameter of 35 mm) from our previous work to verify our hypothesis that the channel actuators should undergo the same shape deformation as their non-channel equivalents. However, the infill pattern had been changed from a honeycomb to a 0-90° square grid to ensure that the channels were interconnected throughout the whole structure and the object was robust and would not collapse.[47,48] Infill density remained the same – 15%. The hydrogel actuator with a core-sheath structure was fabricated by simultaneously extruding (**Figure 1b**) the thermoresponsive filament shell and sacrificial ink (25 wt.% Pluronic® F-127, PF-127 mixed with red food dye) in the core ~~by means of~~employing an 18/22G coaxial nozzle with outer and inner diameters of 832 μm and 416 μm (temperature of 25°C). The nozzle was connected to the two separate printheads, each supplied by a different pressure source (a compressor and a printer). After systematic investigation of ink printability, the printing parameters were optimized to sustain a pressure of 90kPa for the P-127 ink extruded through the inner orifice supplied by a printer, 4.5 bar for the thermoink delivered through the outer orifice pressurized by a compressor, and an overall printing speed of 5 mm/s. The printouts were deposited on a glass Petri dish and subsequently photocured with UV radiation at a wavelength of 365 nm (10 mW cm^{-2}) for 5 min (**Figure 1c, left**), followed by overnight crosslinking with a 0.5M $CaCl_2$ solution (**Figure 1c, right**).

Structural heterogeneity is found in most tissues including vessels.[33] Most hydrogel scaffolds mimicking the mechanical properties and mechanobiological responses of native tissues are designed as heterogeneous architectured materials. However, the mismatch in elastic modulus between materials in a multi-material construct may promptly lead to interfacial mechanical failure. In bilayer soft actuators, a heterogeneous response between stimuli-responsive and non-stimuli-responsive hydrogel layers results in an anisotropic deformation in the bilayer structure upon exposure to a trigger.[39] However, individual layers may rupture and delaminate as the hydrogel swells or shrinks.[49] To overcome this problem, we used a single composite material for the fabrication of homogenous hydrogels. The sacrificial ink (PF-127) was coextruded with thermoink and then removed to create channels. Shear generated during printing induced the alignment of the laponite discs, a viscosity-modifying component of the

ink and nanofiller, along the printing direction resulting in anisotropy within the construct walls.[35] Upon the immersion of the printouts in calcium chloride for alginate crosslinking, the PF-127 core began to dissolve creating lumens and channels (**Figure S1**). We observed that the scaffold changed its color from red to beige which suggested that the colored sacrificial ink was dissolved by the crosslinking solution leaving behind a channel structure within the scaffold as shown in the inset in **Figure 1c**.

Eventually, we obtained a round hydrogel (Coax4Dgel) sheet with a dually (ionically and covalently) cross-linked anisotropic network which was next kept in ultrapure water. Upon immersion in ultrapure water at room temperature, the sheet spontaneously rolled up in the direction of the first printed layer and formed a macrotube.

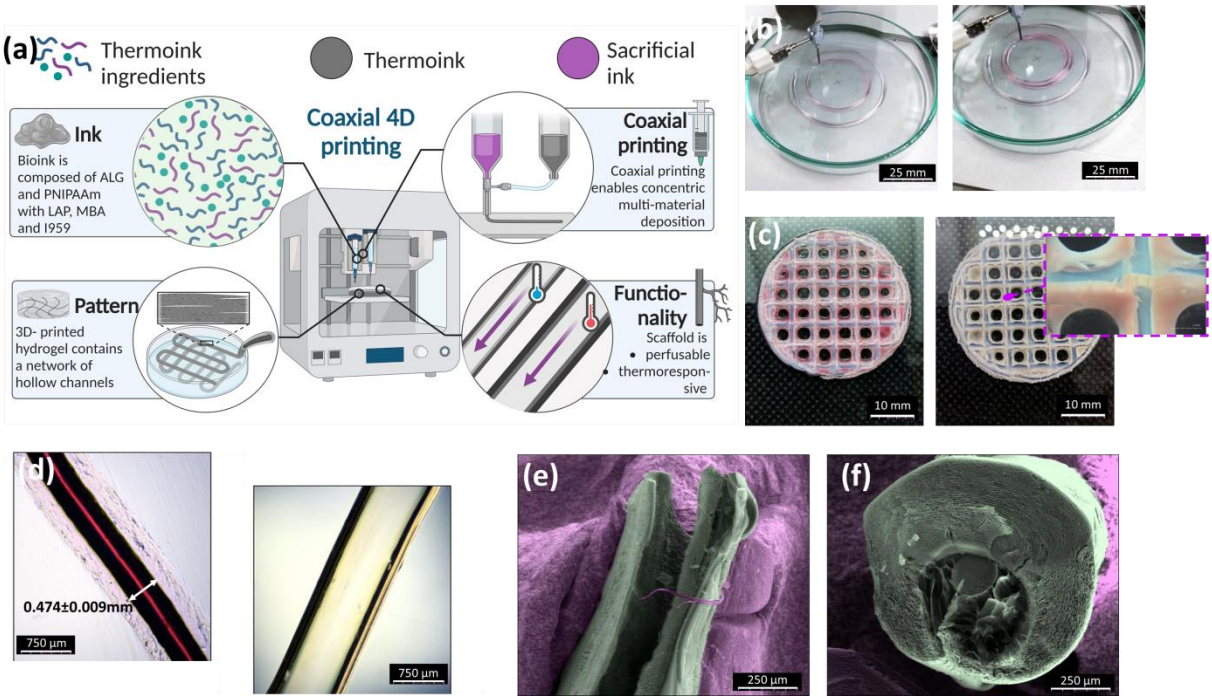

Figure 1. An idea of coaxial 4D printing. (a) Schematic illustration of the study concept; Thermoink and sacrificial material were used for the 4D printing of scaffolds with a network of hollow tubes (channels). The channel hydrogels were permeable and capable of shape-morphing in response to temperature change; (b) Photos of the printing of the thermoresponsive perfusable Coax4Dgel at 25°C; Both thermoink (transparent) and sacrificial ink (purple) are being simultaneously extruded through the coaxial nozzle; (c) 3D-printed and cured channel scaffolds. Coaxially printed filaments interconnect with each other forming vessel-like structures. Inset shows a 10-times magnified image of the channel; (d) An optical image of the coaxially extruded tube; scanning electron microscope (SEM) images of the longitudinal (e) and cross (f) sections of the tube.

To investigate coaxial printing accuracy, we extruded a single tube (~~3 repetitions~~n = 3) and measured its inner diameter right after deposition. (**Figure 1d**). A value of 0.474±0.009 mm was only 12% higher than the nozzle's inner diameter which confirmed high printing accuracy. Scanning electron microscopy reconstructed the three-dimensional microstructure of the hollow fiber (**Figure 1e,f**). The SEM image in **Figure 1e** shows a longitudinal view of the tube which cracked during the SEM sample preparation revealing the porous interior. **Figure 1f** presents a cross-section of another tubular filament having outer and inner diameters of 0.880±0.047 and 0.414±0.022 mm. Although we can see the core-shell structure of the tube, its inside space is not empty, which suggests that in this case, sacrificial ink has not been fully removed from the lumen before preparing the sample for SEM imaging. Nevertheless, we succeeded in fabricating core-sheath/tubular microfibers that can maintain a round section after deposition and crosslinking. Macro- (discs) and microstructures (microtubes) were further used to investigate the temperature-dependent response of the hydrogel.

2.2. Programmable temperature-dependent response

We hypothesized that the size of permeable channels depends on the diameter of the coaxial nozzle, and can be controlled by temperature after printing and cross-linking. To investigate whether the Coax4Dgel microtube can be thermally programmed to change the lumen size or not, a hollow fiber with an inner diameter (ID) of about 0.3 mm (nozzle size of 1.2/0.3mm) was immersed consecutively in four water baths held at 10, 20, 30, and 40°C for 20 minutes under the optical microscope. In this experiment, we also showed that fiber size depends on nozzle size. As shown in **Figure 2a**, the ID of the fiber rose from 0.282±0.017 mm to 0.382±0.020 mm with increasing the temperature from 10°C to 40°C. For the first time, we showed that the lumen size of the hydrogel microtube can be increased even by ~30% simply by changing the temperature of the surrounding medium. Even below the LCST of the Coax4Dgel determined previously at ~32 °C,[36] we observe that the diameter changes thermally in a gradual manner. The lowest shift in the inner diameter (~4%) is observed when the temperature jumps from 20 (0.335±0.016mm) to 30°C (0.348±0.034), but this difference is statistically insignificant (**Figure 2b**). All the other changes in this group are considered statistically significant. We also measured the outer diameter (OD) of the tube (**Figure 2c**) and found that the tendency is similar to that of the ID. The lowest value of 1.354±0.082 mm was achieved for the temperature of 10°C, followed by 1.427±0.039, 1.481±0.027, and 1.508±0.019 mm for 20, 30, and 40°C. Therefore, the difference between the highest and the lowest values is only ~11%, however still significant. The outer diameters of the tube at 30 and 40°C differ insignificantly, which means that in this temperature range, it is possible to

thermally change the lumen size without affecting its overall size. This feature is advantageous, particularly in biomedical applications, where the extensive dimension (volume) expansion is undesirable as it may generate stress on the surrounding tissues when applied *in vivo*.[50]

Figure 2d demonstrates the general mechanism beyond the temperature dependence of the tube lumen size. The molecular interactions between the polymer network inside and water outside the hydrogel are responsible for its thermosensitivity. At temperatures (10, 20, and 30°C) below the LCST of the hydrogel, water molecules migrate into the polymer network and form hydrogen bonds with the amide groups in the polymer backbone. As a result, the matrix hydrates and swells, while the lumen size decreases. Above the hydrogel's LCST (40°C), the hydrogen bonding strength between the polymer chains and the water molecule weakens which leads to the hydrogel dehydration and shrinkage, thereby increasing the diameter of the thermoresponsive tube.[51–53] The tube size is, therefore, controlled by temperature-induced swelling and deswelling of the Coax4Dgel, and the corresponding change of the network volume.[54]

Soft actuators should be designed to withstand multiple actuation cycles and exhibit long-term structural stability. To investigate the structural integrity of our tubes, we repeated the microscopic visualizations and diameter measurements 4 months post-printing (**Figure S2**). Generally, the hydrogels were stable and did not exhibit noticeable degradation. The inner diameters were similar to those of the fresh samples and showed the same temperature dependence. Our Coax4Dgel, therefore, satisfies the stability and functionality requirements of soft robots.

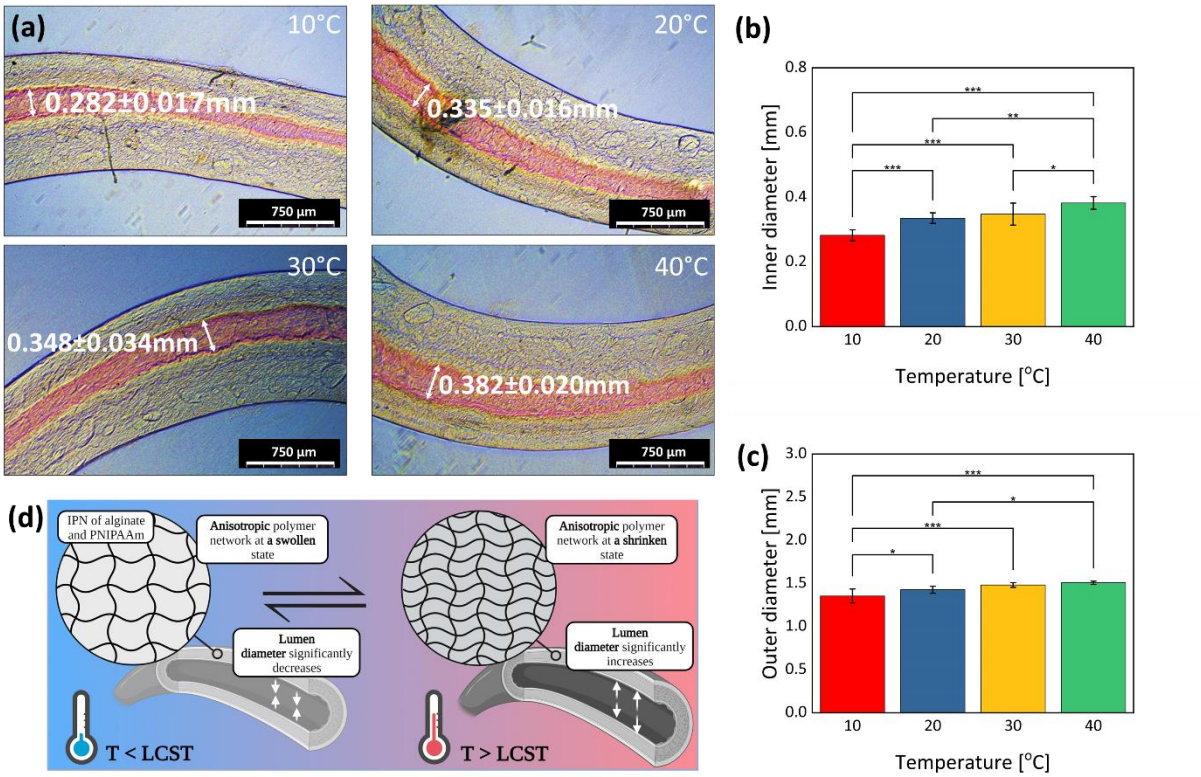

Figure 2. Thermoresponsivity of the coaxially printed microtube. (a) Optical images of the tube kept in water at various temperatures (10-40°C); Tube inner diameter increases significantly with increasing medium temperature; Tube inner (b) and outer (c) diameters as a function of temperature in the range of 10-40°C (n = 10); (d) Schematic illustration of the thermoresponsivity mechanism; Tubes consist of an anisotropic IPN of alginate and PNIPAAm, which swells at a temperature below LCST and shrinks upon heating. This mechanism can be used to control the inner diameter of the tube. * - $p < 0.05$, ** - $p < 0.01$, *** - $p < 0.001$. Statistically insignificant differences were not shown in the plots. Statistical significance was tested with Tukey's and Kruskal-Wallis' tests.

Next, we sought to study the macroscopic thermoresponsivity of the Coax4Dgel. With the previous hypothesis that the shear-induced anisotropy generated during printing drives shape transformation in a single material actuator,[36] we studied the thermal actuation of the coaxially printed hydrogel structures (hollow fibers and discs). First, we examined the microstructure of the printed samples in scanning electron microscopy and determined the pore geometry and orientation angle. Scaffold anisotropy was then assessed by means of OrientationJ, an ImageJ plugin. The Coax4Dgel exhibited an oriented highly porous structure with a dominating orientation angle of ~150° at the top wall of the tube (**Figure 3a and 3b coral arrow**). The percentage of isotropy was only 23.63%, which confirmed the anisotropic nature of the hydrogel's microstructure.

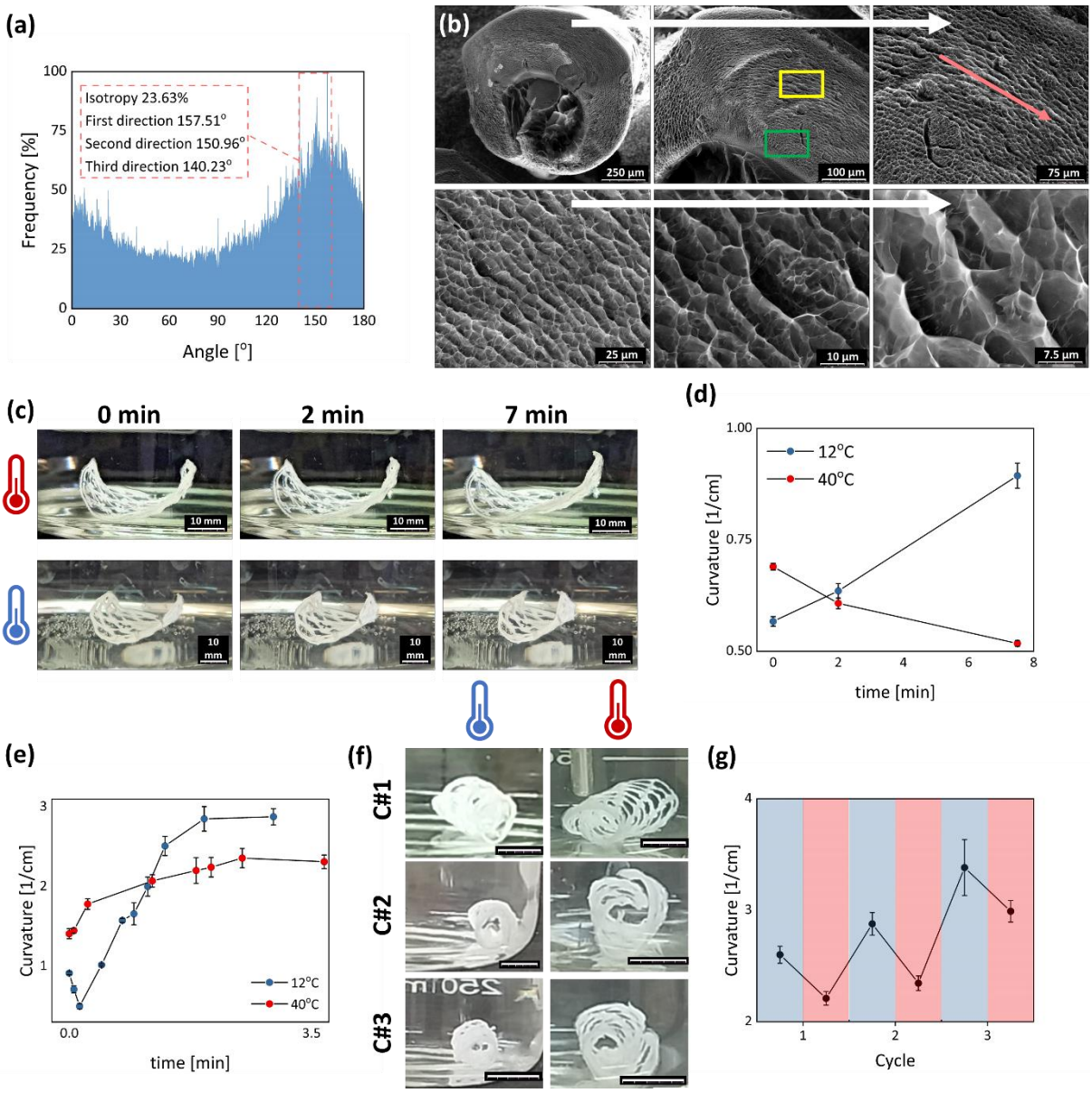

Figure 3. Microstructural anisotropy within the channel/tube wall and macrostructural actuation; (a) Angle distribution of the orientation of polymeric chains in the tube wall of printed Coax4Dgel hollow fiber. The dominating orientation angle (about 150°) is marked as a coral arrow in SEM images (b). Shear stress within the coaxial nozzle induces pore elongation and alignment of the chains. White arrows indicate image magnification. Green and yellow frames are used to mark zones of small and large pores. (c) Reversible shape-morphing behavior of the channel hydrogel discs (3LA) driven by temperature change. The scaffold folds upon cooling (T<LCST) and unfolds when transferred to hot water (T>LCST); (d) The curvature of the 3-layer channel hydrogel as a function of actuation time and temperature (12 and 40°C); (e) The curvature of the 2-layer channel hydrogel as a function of actuation time and temperature (12 and 40°C); (f) photos of the folded hydrogels and (g) the

corresponding plot of bending curvatures in three consecutive heating/cooling cycles. Scale bars correspond to 10 mm.

The SEM images of the tube's cross-section revealed the non-deformed cylindrically shaped fiber having a micron-sized horizontal porous structure with the pores aligning and orientating circuitously around the lumen (**Figure 3b**). The pore system was built up in an ordered manner (hierarchy) with the largest pores of an average size of 41.50±5.80μm in the middle of the tube wall (**yellow frame in Figure 3b**) and the smaller ones (10.18±2.52μm) elsewhere (**green frame in Figure 3b**). The longitudinal alignment of the polymer network walls (SEM image in **Figure 1e**) is thought to be induced by the shear force generated during extrusion. While in-plane photocuring and ionic crosslinking of the network after printing are responsible for the horizontal and hierarchical orientation of the pores.[36,55] The 3D microstructure is then preserved through the freeze-drying of the Coax4Dgel during SEM specimen preparation. Radial structural anisotropy of the hydrogel tube and the fact that larger pores are located in the center of the tube wall may support various cell (e.g. endothelial cells) immobilization. Cells trapped in the large pores would not escape the hydrogel since they may not be able to penetrate smaller voids at the fiber edges. Concomitantly, gases, nutrients, and wastes may freely diffuse in both directions across walls. We found out that our fiber has comparable structural features to the dragonfly wing cross veins which exhibit similar radially oriented microstructure and resulting anisotropy.[56]

All those observations led to the update of our primary hypothesis to match a new (core-shell) hydrogel architecture. We now conjecture that the longitudinally oriented hydrogel network and radially aligned pores render the fiber and consequently the whole structure anisotropic and may lead to stimulus-dependent mechanical response and shape deformation. To test this assumption, we performed temperature-dependent actuation experiments on the 3D-printed channel hydrogel ~~discs actuators~~ having 3 (3LA, **Figure 3c and Movie S1 and S2**) and 2 printed layers (2LA, **Figure S3**). All actuation tests were done in ultrapure water of pH~7.0. We took photos and measured the curvature (**Figure 3d**) of the deforming ~~3-layer shee~~3LA after 0, 2, and 7 minutes of the actuation test. As shown in **Figure 3c and Movie S1 and S2**, the obtained soft actuator (Coax4Dgel sheet) can undergo a clear temperature-responsive out-of-plane bending motion when the hydrogel is consecutively immersed in hot (40°C) and cold (12°C) water baths. In hot water, the ~~3-layer sheet~~3LA shrank and spontaneously unrolled, while its curvature dropped from ~~1.212~~0.690±0.007~~38~~ cm^{-1} at the beginning of the test to 0.~~944~~518±0.00~~4~~7 cm^{-1} after 7 minutes (**Movie S1**). Upon immersion in cold water, the Coax4Dgel actuator with a curvature of 0.~~597~~567±0.010~~1~~ cm^{-1} began to self-fold into a

tubular construct, and in the 7th minute of the test, it reached a curvature of 0.~~709~~894±0.028~~5~~ cm^{-1} (**Movie S2**). Because of the radially aligned pores and hierarchical internal microstructure, the ~~3 layer hydrogel~~sheet swells or shrinks anisotropically. At the microscale, this phenomenon leads to the formation of the local shrunken and swollen zones and corresponding nonuniform strain domains within the hydrogel network.

Based on the previous observations, we assumed that the actuation performance qualitatively measured as curvature strongly depends on the sheet thickness. Since the stretching energy changes linearly, while the bending energy changes cubically with the actuator thickness, the thinner the sheet the higher the performance of the out-of-plane buckling into a 3D shape.[57] The bending curvature of a 2-layer hydrogel vs. time was subsequently measured at 12 and 40°C (**Figure 3e**). Upon immersion in cold water, the hydrogel actuator with an initial curvature of 0.914±0.018 cm^{-1} rapidly unfolded in ~9s reaching a minimal value of 0.499±0.033 cm^{-1}, and then it started to fold in the opposite direction until the stable value of 2.878±0.102 cm^{-1}. When transferred to hot water, the sheet first restored its primary shape and after ~2.5 min stabilized with a curvature of 2.313±0.085 cm^{-1}. Unlike the 3-layer actuator, the 2LA developed a full tube. Besides, the 3LA had twice lower initial and final curvatures and required significantly more time (~7 min) to evolve into the bent-out structure than its 2-layer equivalent (~3 min). We, therefore, showed that actuation performance may be tuned by changing the number of printed layers confirming previous observations.[58]

The hydrogel actuators should not only have high actuation performance but also should exhibit actuation repeatability and structural stability.[59,60] We, therefore, investigated the reversibility and controllability of the shape morphing behavior of 2LA by measuring the bending curvature consecutively in 12 and 42 °C (**Figure 3f**). In three cycles, ~~T~~the shape transformation of the hydrogel activated by temperature was reversible and repeatable (**Figure 3f,g**), and the sheet remained stable without any obvious change. The curvature of the 2LA insignificantly increased over cycles from 2.60 ± 0.076 cm^{-1} to 2.99 ± 0.096 cm^{-1}, as a consequence of the leakage of unreacted components or hydrogel softening under cyclic deformation.[36,61]

Out-of-plane bending at a temperature below the LCST of the hydrogel is achieved by relieving in-plane internal non-equilibrium stress generated by this swelling differential under external stimuli[62,63]. This shape-morphing behavior is aided by increased local water delivery through the channels resulting in nonuniform overall hydration; hence, swelling of the Coax4Dgel actuator.[64] The process is reversible as the sheet can be unfolded by removing the differential in swelling within the hydrogel, which occurs at a temperature above its lower

critical solution temperature (LCST).[65] We, therefore, demonstrated that the 3D-printed channel hydrogel capable of shape-changing under external triggers may serve as a novel perfusable bioactuator towards active implantology (e.g. engineered muscle tissue) and vascularized soft robots.

2.3. Multifunctionality and perfusability

Channels and tubes can be used in engineered living materials (ELMs) to dynamically supply nutrients and gases through the lumen to cells immobilized within the hydrogel network.[66] In core-shell systems with a central axis laden with microorganisms, a shell made of a dense polymeric hydrogel matrix may serve as a barrier protecting the cells from environmental effects and preventing them from leaking into the surroundings.[67,68] Here, for the first time, both problems are solved with the aid of coaxial printing. We show that microorganisms can be directly encapsulated within the three-dimensional (3D) hydrogel Coax4Dgel core (**Figure 4a**) or sheath (**Figure 4b**) of the core-shell microfilaments paving the way to new 3D-printed multi-functional ELMs having functions of both living microorganisms and stimuli-responsive polymers. We used microalgae *Chlamydomonas reinhardtii* strain CCAP 11/32A as a fluorescent probe to demonstrate the coaxial printability and shape fidelity of Coax4Dgel with or without embedded cells by fabricating tubular or core-sheath constructs. Microalgae viability can be easily visualized under fluorescent microscopy due to the autofluorescence emitted from chlorophyll molecules of a chloroplast in their cells at 680 nm.[69] First, we formulated microalgae-containing ink (M#1) by adding microalgae suspension (1.3×10^6 cells/ per ml of Tris-Acetate-Phosphate (TAP) medium) to the thermoink, which was further coprinted with sacrificial ink as a tube with an 18G/22G nozzle and printing pressure of 40kPa/4.0bar and then UV and ionically crosslinked. In the second approach, microalgae-embedding ink (M#2), a mixture of 6wt.% LAP and 1wt.% ALG in 10ml of TAP medium and water 1:1 solution with 1mL of microalgae suspension (1.3×10^6 cells/ml) was coextruded with the thermoink in the form of a core-shell microtube using an 18G/22G nozzle and printing pressure of 45kPa/4.5bar followed by photo- and Ca^{2+}-curing. The rheological properties (the storage (elastic) modulus (G') and loss (viscous) modulus (G") versus strain amplitude at a fixed angular frequency) of sacrificial and M#2 inks were shown in **Figure 4c**, while those of the thermoink had been demonstrated previously. The strain sweep testing plots of SI and M#2 exhibited the viscoelastic region for strains lower than ~6 and 22%. Within those regions, G' dominates over G", confirming that the elastic portion of the viscoelastic behavior prevailed. When the cross-over points (critical strains) were reached (G'=G"), G" became greater than G', which was attributed to the dominance of the viscous

portion of the viscoelastic behavior (**Figure 4c1**). The inks reversibly transited from gel to viscous liquid. Such viscoelastic properties of the materials are highly desired for direct printing as it ensures the extrusion accuracy and 3D shape fidelity of the printed objects.

We then demonstrated that the thermoink is highly printable ~~by means of~~employing a coaxial nozzle and can be used to manufacture two types of core-sheath materials presented in **Figure 4a,b**. As shown in **Figure 4a1**, microalgae cells are only immobilized within the tube wall and are not observed in the core since it is hollow (Mgel #1). We believe that such geometry could be further used to oxygenate the perfusing medium through the photosynthetic activity of microalgae. **Figure 4b1** presents a fluorescence image of the microalgae encapsulated within the alginate core surrounded by the Coax4Dgel, where microorganisms were not detected (Mgel #2).

Next, we investigated the stability of microorganisms immobilized within our constructs by fluorescence microscopy. Determination of cell viability proved not easy since encapsulated cells are difficult to quantify directly because they are embedded within a dense 3D hydrogel matrix with slight autofluorescence interfering with the signal from cells. However, a grid method and ImageJ's Analyze Particles command enabled us to count the number and measure the diameter of live cells per 0.2×0.2 mm square and take their fluorescence images on the 1st, 3rd, 5^{th,} and 7th day of incubation in a TAP medium under red light (dark/light phases) at room temperature (**Figure 4d,e**). We found out that at the beginning of culturing (**Figure 4d1**), microorganisms in Mgel #1 formed colonies whose average diameter on Day 1 was ~35% higher (17.66±8.45 μm) than that measured on Day 5 (11.21±6.14 μm). The difference was statistically insignificant, meaning that the colony-forming tendency had no impact on the overall cell viability. The difference in the cell number per 0.2×0.2 mm grid between Day 1 and Day 5 was statistically irrelevant. **Figure 4e1** shows that the cells encapsulated within the alginate core of Mgel #2 were evenly distributed, and no cells were found exterior to the tubes over 7 days of incubation. The differences in cell number and size measured at each of the 7 days were statistically insignificant, which suggested a stable cell culture. The same colony-forming tendency as for Mgel #1 was observed on Days 1 and 3 with average colony diameters of 16.98±10.75 and 16.97±9.06 μm, which then dropped by ~15% on Day 7 (14.33±6.97μm). Altogether, these results confirmed that Coax4Dgel has no impact on cell viability, but hinders cell leakage through the shell. When combined with coaxial printing, it is an effective tool to immobilize and integrate engineered living matter with stimuli-responsive polymeric materials into multifunctional core-shell constructs as shown in **Figure 4f**. A disc with a flower-like geometry and microalgal central paths was

created with Coax4DIP and Mgel#2. Microalgae were able to survive for 5 days of incubation in a TAP medium when encapsulated within the hydrogel 3D constructs, which confirmed their high entrapping potential. We, therefore, proved that with this technology one can produce constructs that are nearly unlimited in terms of shape or architecture with possible applications in tissue engineering, soft robotics, and regenerative medicine.

Next, we used a microalgae medium to perform permeability tests on our microtubes (**Figure 5a1**). We hypothesized that microalgae were small enough to move freely through the lumen, but large enough not to penetrate the hydrogel wall as it might occur for fluorescent dyes. The microalgae suspension at 20°C was injected into the core/lumen of the previously printed thermoresponsive tube under the fluorescent microscope. As shown in **Figure 5a2~~b~~** and **Movie S3**, *Chlamydomonas reinhardtii* cells with an average size of ~10μm diffused freely and efficiently through the microtube upon reaching the outlet. The diffusion lasted ~26s, starting from the injection (0s) and ending when the cells began to exit the tube (26.51s) (**Figure 5b1**). Time should be doubled since **Movie S3** is sped up twice. The relationship between the normalized perfusion distance and perfusion time of microalgal suspension is presented in **Figure 5b2**, where one unit corresponds to ~0.7cm. Microalgae only diffused lengthwise and neither radial movement nor diffusion across the Coax4Dgel wall was observed.

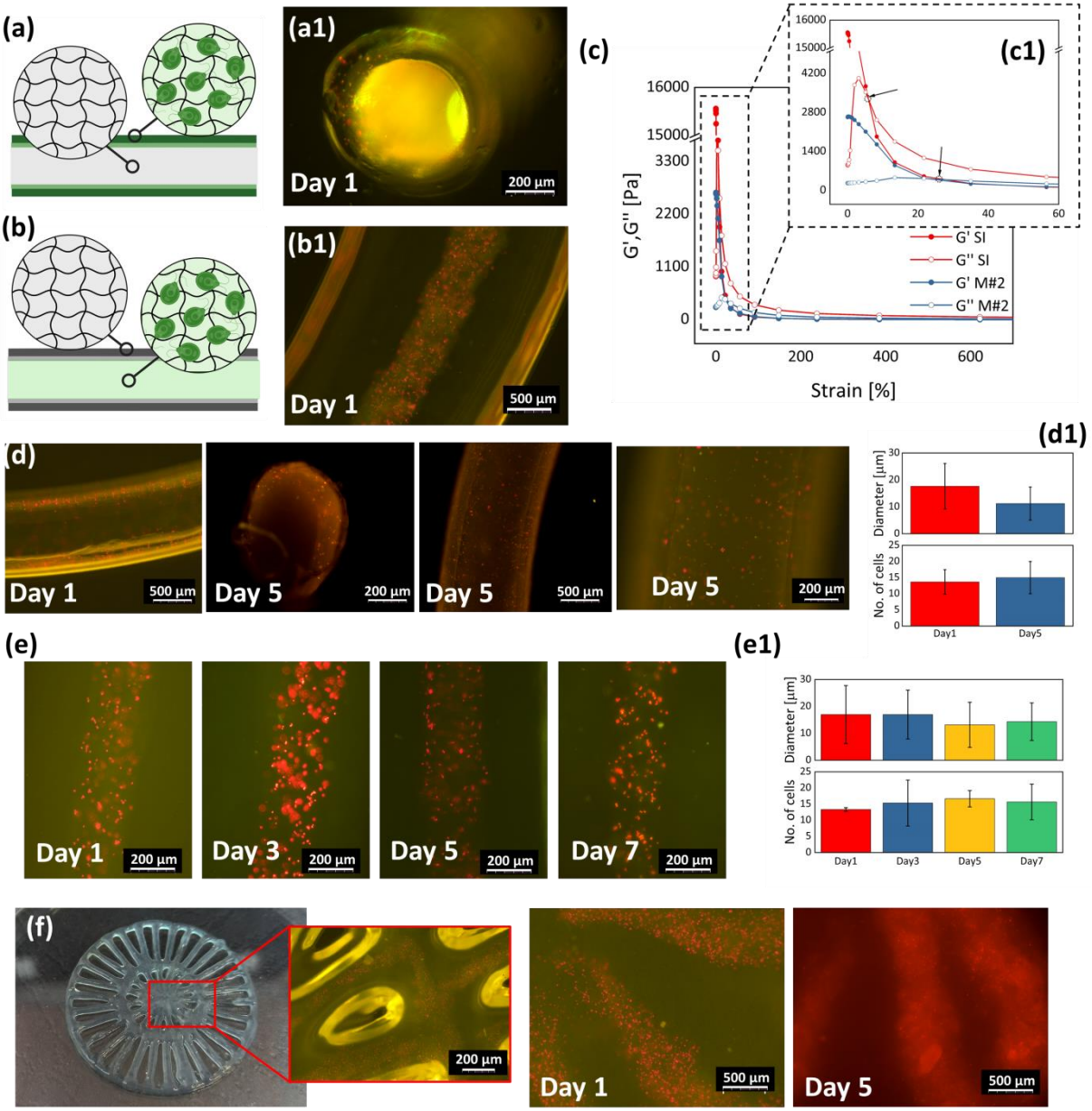

Figure 4. The microalgae-assisted visualization of coaxially 4D-printed thermoresponsive Coax4Dgel tubes; (a) and (b) present the printability of thermoink. Microalgae serve as an autofluorescent indicator. Thermoink can be delivered through both inner and outer nozzles forming a tube core (a) and shell (b); (a1) Fluorescence image of photosynthetic cells immobilized within the thermoink (microalgal ink #1) extruded as a sheath. A core is composed of PF-127; (b1) Fluorescence image of the microalgae-laden core. The coaxial nozzle enables simultaneous extrusion of two types of inks, composed of microalgae *Chlamydomonas reinhardtii*-laden alginate (microalgal ink #2) and the IPN of ALG and PNIPAAm, during single printing. (c) rheology of the inks – storage, and loss moduli vs. strain for sacrificial (SI) and M#2 inks. Inset (c1) shows cross-over points corresponding to G' = G"; before it G"<G' (solid-state) and after G" > G' (fluid state). (d) Images confirming high

microalgae viability in Coax4Dgel shell over time (5 days) (Mgel #1); (d1) A plot comparing microalgae size (average cell diameter) and viability (number of cells per 0.2×0.2 mm grid~~, 5 repetitions~~n = 5) on 1st and 5th day of culturing in the core-shell constructs. No significant differences are reported; (e) Images confirming high microalgae viability in the alginate core over time (7 days) (Mgel #2); (e1) A plot comparing microalgae size (average cell diameter) and viability (number of cells per 0.2×0.2 mm grid, ~~3 repetitions~~n = 3) on 1st, 3rd, 5th, and 7th day of culturing in the core-shell constructs. The results were not significantly different. (f) The combination of thermoink and microalgal ink #2 in a coaxially printed 3D construct. The cells survived 5 days in the scaffolds. * - $p < 0.05$, ** - $p < 0.01$, *** - $p < 0.001$. Statistically insignificant differences were not shown in the plots. Statistical significance was tested with Tukey's and Kruskal-Wallis' tests.

Next, we analyzed the interconnectivity and perfusability of the channel macrostructure by injecting the microalgae suspension directly into the Coax4Dgel sheet (**Figure 5c1~~d~~**). Fluorescent imaging enabled the visualization of cells perfusing within the channels with an average diameter of 0.430±0.065 mm. The ~~elliptic fourth~~ image in **Figure 5c2** was taken in a backlit mode to visualize hydrogel being perfused by a microalgae medium. As demonstrated in **Figure 5d1e**, the needle was inserted straight through the hydrogel wall into the empty canal (white dashed frame), followed by the microalgal medium delivery (lighter red zones). The pseudo-coloring technique (**Figure 5d2**) was used to qualitatively and quantitatively present perfusion in channels. While the colors themselves do not carry inherent numerical values, they are assigned to indicate levels of perfusion. Red and yellow represent areas with high medium flow, while light green and blue indicate lower perfusion. The flow started within 2.57 s of needle insertion (**Movie S4~~3~~**). Fluid pressure upon injection drives the flow forward. After 5.70s since the onset of the process, the whole structure was filled with the cell medium. **Figure 5e~~f~~** presents the continuation of the cell diffusion through the hydrogel matrix, thanks to its interconnected channel structure and high permeability. No cell escape through the walls was observed. By examining the distribution of the fluorescent signals, we confirmed that microalgae flowed through the entire scaffold (**Figure 5f~~g~~**) and were only present in the voids not within the hydrogel pores.

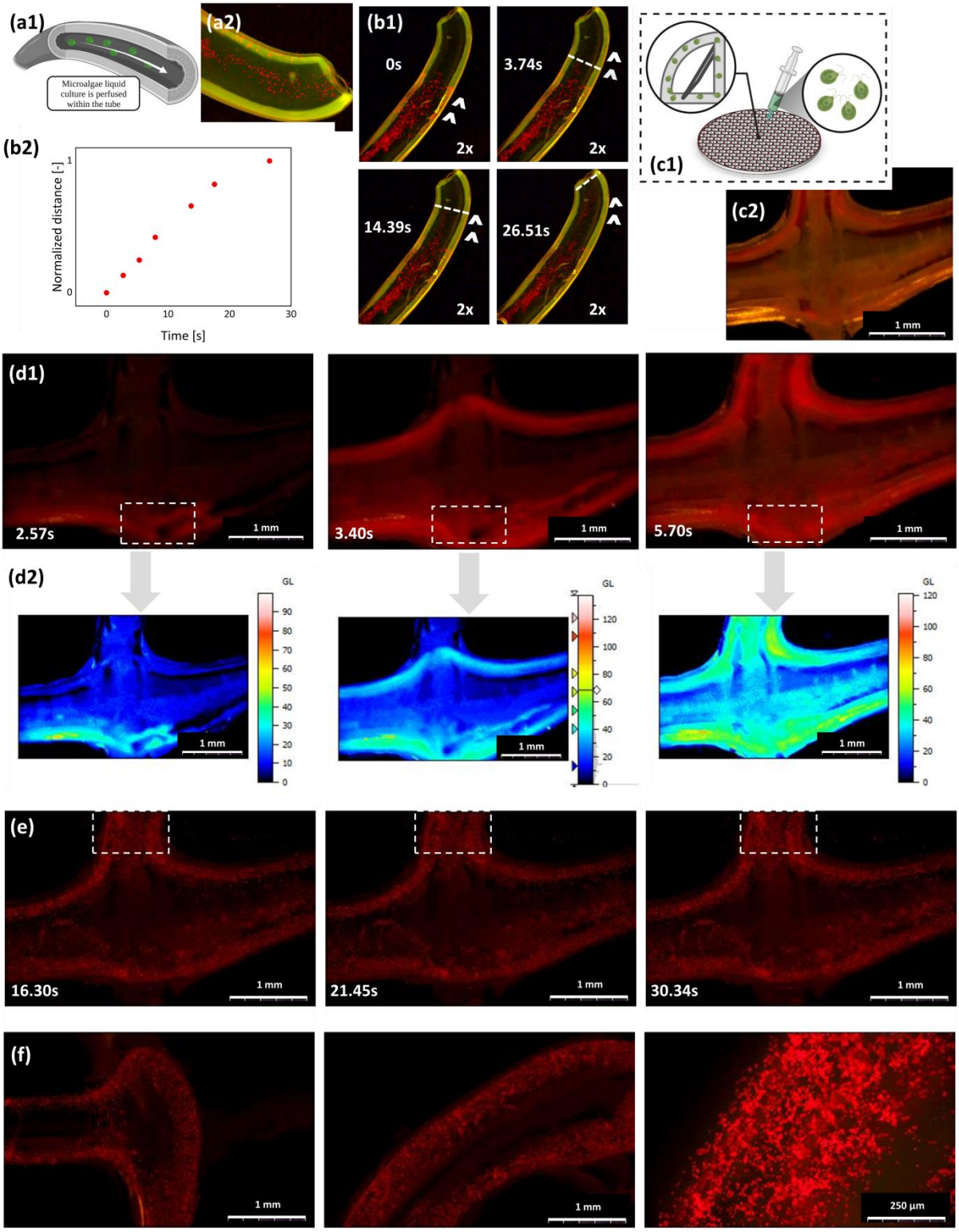

Figure 5. Perfusability of the tube and channel scaffold; (a1) Schematic concept of the study of the tube perfusion rendered through microalgal autofluorescence; (a2) Microalgae flowing in the core confirms that the tube is permeable; (b1) Microalgae diffusion in the channel over time. After ~26 s (sped up twice) microalgae reach the tube outlet; (b2) quantitative analysis of medium diffusion within the tube – a plot of a normalized distance vs. time; one unit corresponds to ~0.7cm; (c1) The concept of the scaffold permeability test and (c2)

fluorescence visualization of channel network in the thermoresponsive hydrogel being perfused with microalgae solution. (d1) The microalgae-containing solution is injected (white dashed frame) into the Coax4Dgel channels and its perfusion is observed under the fluorescence microscope; (d2) shows pseudocolored images with a numeric scale normalized to 100 of the perfusing medium; (e) Microalgae diffusion in the channels over time, which is the most apparent in the location in the dashed frame; (f) Microalgae are seen in the interconnected channels throughout the whole structure. The last image shows the magnification of the channel embedded with photosynthetic cells.

2.4. Biocompatibility

Most soft robots rely on elastomeric materials having limited cytocompatibility to serve reliably in biomedical and tissue engineering applications. The difficulty with biocompatibility can be, however, overcome by replacing elastomers with cytocompatible stimuli-responsive hydrogels like the one investigated in this study (Coax4Dgel). Previous studies already proved the biocompatibility of the PNIPAAm-ALG system when employed for biofabrication of temperature-triggered injectable-hydrogel-based wound dressings and tissue models.[70,71]

Besides, hydrogels mimicking the vein-like systems must be supportive of endothelial cell ~~(EC)~~ growth. These biological characteristics of the Coax4Dgel were evaluated with Immortalized Human Vascular Endothelial Cells (EA.hy926) (**Figure 6**), one of the main EC lines that actively participate in angiogenesis.[72] The cells were seeded on a hydrogel surface at a density of ~1.3×10^4 cells/cm^2.

To investigate the effect of our Coax4Dgel on cell growth, we quantified the percentage viability during a 5-day culture in the presence of the hydrogel (S) (**Figure 6a**). EA.hy926 viability was calculated over time with respect to the experimental control (C) which were cells cultured without the presence of hydrogel. After 24 hours of incubation, hydrogel exhibited no toxicity based on an EC viability test in which the cell survival rate was 93.1±7.60%. The difference between the sample and the control was statistically irrelevant. In the next 24 hours, the EA.hy926 viability significantly improved and reached a value of 107.2±1.08%, being irrelevantly higher than that of the C. This improvement was maintained till the 5th day of the culture achieving 108.9±1.68% viability. The Live/Dead staining in **Figure 6b** revealed a few dead EA.hy926 cells confirming high cell viability.

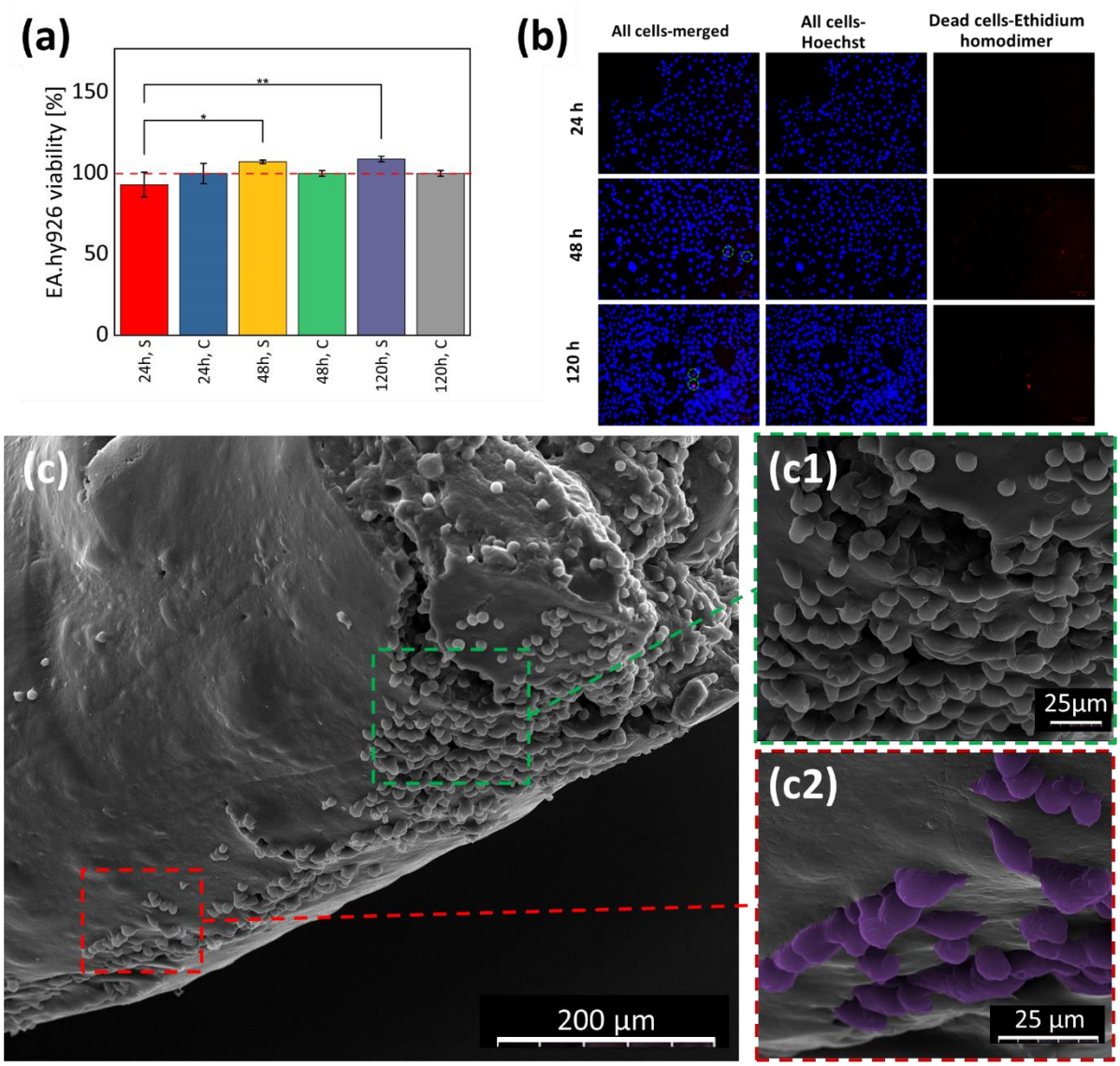

Figure 6. Cytotoxicity and biocompatibility of coaxially printed hydrogel toward endothelial cells (*in vitro* test*)*; (a) Quantitative EA.hy926 cell viability. S and C correspond to the sample and control. The red dashed line indicates 100% viability (n = 4); (b) Cell viability (Live/Dead assay) on endothelial cells. Cell death was determined by Hoechst and Ethidium Homodimer-1 double fluorescent staining. The blue channel depicts all cells, while the red channels depict dead cells; (c) and (d) present SEM images of EA.hy926 cells after culturing on the thermoresponsive tube surface for 120h. In (d), cells attached to the hydrogel are colored violet. * - $p < 0.05$, ** - $p < 0.01$, *** - $p < 0.001$. Statistically insignificant differences were not shown in the plots. Statistical significance was tested with Tukey's and Kruskal-Wallis' tests.

As reported previously, human umbilical vein endothelial cells exhibited stable and firm adhesion to the PNIPAAm-based hydrogel surface.[73] The attachment was regulated primarily by the surface roughness controlled by the crosslinking density of the PNIPAAm hydrogel

and the surrounding temperature around the PNIPAAm's LCST (32°C). The cells readily adhered to the surface at a temperature above the LCST and detached when it dropped to 20°C. This process was found to be driven by the change of hydration degree and corresponding surface topography as high water content and rough surface hindered effective cell adhesion.[74] Following these observations, we qualitatively examined the attachment of EA.hy926 cells to Coax4Dgel by SEM imaging. The biocompatibility tests were performed at 37°C, which is a few degrees higher than the volume phase transition temperature of Coax4Dgel. Therefore, we hypothesized that ECs stably adhered to the hydrogel surface. This phenomenon should be additionally aided by the presence of biocompatible alginate. The structure was further preserved during SEM sample preparation steps including fixing in 2.5% glutaraldehyde, draining with a graded series of ethanol (50-98%), and air drying for 3 days. EA.hy926 cells were attached to the surface of hydrogel, but the coverage was non-uniform as shown in **Figure 6c**. The cells adhered where the wrinkles or creases were present. Magnified SEM images in **Figure 6c1-c2** revealed that the cells are abundantly attached to the hydrogel surface. These results, however, are not sufficient to propose the mechanism of EA.hy926 adhesion on the Coax4Dgel surface. A more advanced study is, therefore, necessary to quantitatively determine cell attachment and detachment from the hydrogel in a wide range of temperatures.

As shown previously, a similar microchannel PNIPAAm-based scaffold can be successfully used for easy and rapid microscale vasculature fabrication in thermoresponsive hydrogels using their capability to shrink at a physiological temperature.[75] We, therefore, believe that ~~Altogether, these results confirm that~~ Coax4Dgel ~~is nontoxic to endothelial cells and~~ can be further explored *in vivo* for biomedical applications in soft robotics (e.g. artificial muscle) and vascular tissue engineering since it is nontoxic to endothelial cells.

3. Conclusion

In this paper, a bioinspired thermoresponsive hydrogel scaffold with a network of arranged channels and oriented microstructure has been designed and fabricated ~~by means of~~using a new printing strategy. We proposed coaxial 4D direct ink printing which combines coextrusion printing with materials capable of shape-changing in response to external triggers. Using Coax4DIP, a channel-embedded hydrogel was fabricated by shaping the coaxially printed microtubes into a sheet actuator of a designed geometry and the capability of thermal actuation. We showed that the diameter of the single microtube can be tuned dually (pre- and post-printing) by changing the nozzle size and through temperature-dependent swelling/deswelling of the hydrogel. The microtube exhibited radial and longitudinal

microstructural anisotropy which guided out-of-plane deformation of the macrostructure (the soft actuator), leading to its self-folding and unfolding motions around the lower critical solution temperature (LCST) of the hydrogel. The channels enhanced this process by increasing the rate of the hydrogel's hydration from the inside. Both the microtubes and channel structures were permeable and supported the endothelial cell growth as confirmed by cell viability. We believe that our channel thermoresponsive actuator lays the foundations for multi-functional robots equipped with perfusable and adaptable circulatory systems. We, therefore, anticipate the adoption of Coax4DIP in the future printing of different types of smart/stimuli-responsive hydrogels.

Finally, we showed that Coax4DIP can be used to produce a new photosynthetic engineered living material based on microtubular constructs with microalgal cells immobilized either in the core or shell. The hydrogel prevented the cells from escaping to the surrounding medium and supported their growth when cultured for 5-7 days. This study will be extended by a comprehensive investigation of photosynthetic activity and oxygenation efficiency of microalgae encapsulated in core-shell and channel constructs. Nevertheless, our findings pave the avenue for the next generation of ELMs with a system of perfusable veins being highly attractive for a myriad of biomedical and bioengineering applications.

We envision that this approach can be extended to other inks broadening the range of applications from biomedicine, through soft robotics, to engineered functional materials.

4. Experimental Section

Cultivation of microalgae: The microalgae *Chlamydomonas reinhardtii* strain CCAP 11/32A culture was carried out for 7-14 days at a temperature of ~25°C in a day-night (12h) periodic operation system (light phase - dark phase). The light source was provided by an LED panel dedicated to plant cultivation. Mechanical agitation on an orbital shaker (110 RPM) ensured adequate circulation of the culture medium. Cells were visualized under a fluorescence microscope (Leica DMi8 Microsystems) equipped with FITC and Cy3 filters. Measurement of fluorescence intensity was done using 480 and 680 nm as excitation and emission wavelengths.

Formulation of the inks: Thermoink was formulated in a procedure previously described.[36] Briefly, a monomer N-isopropylacrylamide (NIPAAm, Sigma Aldrich, Germany, purity 97%) (10 mmoles, 1 eq.), of a crosslinker N,N-methylenebis(acrylamide) (MBA, Sigma Aldrich, Germany, purity 99%) (0.6 mmoles, 0.06 eq.), and of a photoinitiator 2-hydroxy-4-(2-hydroxyethoxy)-2-methylpropiophenone (Irgacure 2959, I2959, Sigma Aldrich, Germany, purity 98%) (0.5 mmoles 0.05 eq.) were dissolved under stirring (400 RPM) in degassed and

filtered ultrapure water (10 mL) (pH~6-7) maintained at 25 °C. Subsequently, the stirring speed was increased to 1500 RPM to create a vortex, and laponite XLG (LAP, BYK Additives & Instruments) (0.6 g) was gradually added to the solution and allowed to homogenize and form pregel, followed by the addition of sodium alginate (ALG, M_w ~ 120 000–190 000; M/G ratio 1.56, Sigma-Aldrich, Germany) (0.1 g). Finally, the pregel was treated in an ultrasonic bath for 10 min. A microalgal cell (1.3×10^6 cells/ml) suspension (1mL) was added to the thermoink to formulate the microalgae-containing ink #1.

Sacrificial ink was formulated by dissolving Pluronic® F-127 (PF-127, Sigma Aldrich, Germany) (2.5g) in ultrapure water at 8-12°C in a thermostated water bath under stirring (400 RPM). A drop of red food dye was then added to the solution for visualization of the core-shell structure.

The microalgae-containing ink #2 was prepared by mixing microalgae (1.3×10^6 cells/ml) suspension (1mL) with 6wt.% LAP and 1wt.% ALG in Tris-Acetate-Phosphate (TAP) medium and water 1:1 solution (10 mL) under sterile conditions.

The inks were then poured into 3 mL UV-shielded syringes, and centrifuged to remove air bubbles for 10 min at room temperature and 5800-6500 RPM.[5]

Rheology: The rheological characterization of the inks was conducted by means of a plate-plate rheometer (Anton Paar MRC 302, Graz, Austria), with a 25 mm diameter plate. The tests were performed at a fixed frequency of 1 Hz within a strain range of 0.01–1000% and at room temperature.

Coaxial 4D printing: Filled cartridges were placed in the bioprinting machine (CELLINK BIO X 3D printer, BICO, USA and Sygnis S.A., Poland). The 3D objects were designed in CAD software (Inventor) and exported to a GCODE file format acceptable by the printing device.

Thermoink and the sacrificial ink were pneumatically co-extruded through coaxial 18G/22G (832/416 μm) and 1.2/0.3 mm nozzles onto a temperature-controlled substrate along the designed path at room temperature into a microtube and a sheet actuator with 0-90° grid pattern and infill density of 15%. The temperature was maintained at 25°C. The printing parameters were as follows: printing speed: 5 mm/s, printing pressure: 4.5 bar supplied by the air compressor (Airmaster 200/8/24) to the outer nozzle, and 90kPa delivered by the bioprinter to the inner nozzle. Both pressure sources were connected to the bioprinter's printheads. Completed printouts (microtubes and sheets) were cured under UV light (10 mW cm^{-2}, 365 nm) for 5 min followed by immersion in 0.5M $CaCl_2$ for 24 h for PNIPAAm and alginate crosslinking. After washing several times with 96% ethanol (Sigma Aldrich,

Germany) and water to remove unreacted species, the samples were plunged into ultrapure water and left for the next analyses.

Microalgae coaxial 4D printing: Two approaches were used to fabricate cell-laden microfilaments: (1) the microalgae-containing ink #1 (M#1) was coextruded with sacrificial ink in the form of a core-shell microtube; (2) the microalgae-containing ink #2 (M#2) and thermoink were simultaneously deposited to obtain a core-shell microfiber. Printing was realized with an 18G/22G nozzle and a printing pressure of 40kPa/4.0 bar and 45kPa/4.5bar for M#1 and M#2, respectively. Subsequently, the printouts were cross-linked. Next, the scaffolds were placed in TAP medium and maintained under red light for the next 5-7 days. Cell viability and size within 5- and 7-day periods were assessed using ImageJ's Analyze Particles command (n = 3 and 5).

SEM visualization: Before SEM imaging, the microtubes were placed on a cryogenic stage, and plunged in liquid ethane, followed by freeze-drying. The cross- and longitudinal sections of the hydrogels were visualized with a scanning electron microscope, Quanta 250 FEG 1.

The EA.hy926 seeded scaffolds were fixed with 2.5% glutaraldehyde (Sigma Aldrich, Germany) solution for SEM studies, then drained with a graded series of ethanol (50, 75, 90, and 98%) and allowed to air dry for 3 days. Thereafter, to assess cell morphology and adhesion. Samples were coated with metal and examined by SEM (FEI Quanta 200 FEG).

Temperature-dependent tests: The 3D-printed microtubes were consecutively immersed in water (pH~7) baths kept at 10, 20, 30, and 40°C in a cryostat (Julabo FB50) for 20 minutes. Next, the samples were imaged in the bright-field mode under the fluorescent microscope. The outer and inner diameters were measured with ImageJ and the average value (n = 10) was calculated.

Thermal actuation: The thermal actuation test was also performed in the cryostat. The hydrogel sheet was consecutively immersed in heated (40 °C) and cooled (12 °C) water (pH~7) for 20 minutes. At 0, 2, and 7 minutes, the photo of the shape-morphing structure was taken. The 2D bending curvatures (n = 3) were determined as previously described by calculating the inverse of the radius of the osculating circle drawn on the front-view images obtained through a Kappa plugin for ImageJ. A film of the bending motion of the sheet was recorded by the camera.

Permeability tests: The permeability was tested by injecting the microalgal suspension with a concentration of 1.3×10^6 cells/ml (~100µl) into the microtube lumen or hydrogel channels with a 30G nozzle under the fluorescence microscope. The suspension was left to perfuse and diffuse along the channels as driven by the concentration difference and injection pressure.

The fluorescent images of the flowing medium were taken at different time points to describe the perfusion kinetics. A film of the perfusing solution was recorded by the microscope.

Endothelial cells EA.hy926 and material seeding: Endothelial EA.hy926 cells were maintained with Dulbecco's Modified Eagle Medium (high glucose), supplemented with 10% FBS, 100 µg/mL Penicillin, 100 U/mL Streptomycin (Thermo-Fisher Scientific, Waltham, MA, USA), in a humidified CO_2 chamber (37°C, 5% CO_2). For cell culturing, protocols provided by the supplier were followed. Cells from passages 10 to 12 were used in this study. Samples of the Coax4Dgel were fabricated using the above-mentioned protocols, followed by washing three times alternately with autoclaved ultrapure water and 96% ethanol. Next, the samples were UV-sterilized (2 hours), washed three times with DPBS, and incubated for one day with the appropriate cell culture medium before cell seeding. For cell ~~related~~ experiments, we used samples within the time of 24 - 48 hours post-printing. The next day, cells were seeded into 48-well (CELLSTAR®, VWR, Netherlands) or 8-well Millicell EZ SLIDE glass plates (Merck, Kenilworth, NJ, USA) on a hydrogel surface at a density of ~1.3×10^4 cells/cm^2. Cell culture medium was then added to each well, and the plates were moved to a cell incubator (37 °C, 5 wt. % CO_2). The medium was changed daily.

Viability and staining of EA.hy926: To determine the viability of EA.hy926 seeded on the hydrogel surface, samples corresponding to different time points (24, 48, and 120 h) were treated with CellTiter 96® Aqueous One Solution Cell Proliferation Assay (MTS, Promega). For this purpose, the cell medium was removed from the wells, and 100 µL of DMEM and 15 µL of MTS reagent were added and incubated at 37°C for 3 hours. Following the reaction, the recovered supernatant was moved to another 96-well plate and the sample's absorbance was read at 492 nm (Epoch, BioTek®, USA). Cell viability was calculated over time with respect to the experimental control (cells cultured without the presence of hydrogel) to normalize the absorbance (Abs) of each experimental group. Viability of the cells was reported based on 4 investigated samples (n = 4).

$$Viability = \frac{Abs\ of\ sample}{Abs\ of\ control} \times 100\%$$

To more comprehensively study the viability and distribution of cells cultured with hydrogels, Live/Dead staining was performed. Firstly, samples were washed with DPBS and incubated with Ethidium-1 homodimer (10 µM) and Hoechst (10 µg/ml) at 37 °C for 45 minutes. Secondly, a washing step with DPBS was performed and cells were fixed with paraformaldehyde (PAF, 4%). Finally, the cell viability was examined with a fluorescence

microscope (ZOE, Biorad, Hercules, CA, USA). Microphotographs revealing live cells as blue and dead cells as red were taken randomly during an inspection.

Statistical analysis: Measurements were repeated at least three times (information on sample size (n) is added in each section) and the results were expressed as a mean ± standard deviation (SD). Statistical significance was tested with Tukey's and Kruskal-Wallis' tests in OriginPro 9.7 software and was declared as significant (*) at $0.01 \leq p \leq 0.05$, (**) at $p \leq 0.01 \leq 0.001$, and (***) at $p \leq 0.001$. Statistically insignificant differences were not shown in the plots.

Supporting Information

Supporting Information is available from the Wiley Online Library or from the author.

Conflict of Interest

The authors declare no financial or commercial Conflict of Interest.

Data Availability Statement

Data is available on request from the authors.

Acknowledgments

The study was financed by the Polish National Science Centre (Grants No. 2016/23/D/ST8/01267 and 2016/21/D/ST8/01713). D.P. acknowledges the support from the Academia Iuvenum, Wrocław University of Science and Technology. J.S.S. gratefully acknowledges the support of a grant from the FNRS (FNRS-Aspirant, Grant No. FC 46599).

Received: ((will be filled in by the editorial staff))

Revised: ((will be filled in by the editorial staff))

Published online: ((will be filled in by the editorial staff))

References

[1] S. Panda, S. Hajra, P. M. Rajaitha, H. J. Kim, *Micro and Nano Systems Letters* **2023**, *11*, 1.

[2] W. Sun, A. S. Williamson, R. Sukhnandan, C. Majidi, L. Yao, A. W. Feinberg, V. A. Webster-Wood, *Adv Funct Mater* **2023**, 2303659.

[3] J. R. Aggas, S. Abasi, J. F. Phipps, D. A. Podstawczyk, A. Guiseppi-Elie, *Biosens Bioelectron* **2020**, *168*, 112568.

[4] J. Simińska-Stanny, M. Nizioł, P. Szymczyk-Ziółkowska, M. Brożyna, A. Junka, A. Shavandi, D. Podstawczyk, *Addit Manuf* **2022**, *49*, 102506.

[5] D. Podstawczyk, M. Nizioł, P. Szymczyk, P. Wiśniewski, A. Guiseppi-Elie, *Addit Manuf* **2020**, *34*, 101275.
[6] Y. Zhao, C. Xuan, X. Qian, Y. Alsaid, M. Hua, L. Jin, X. He, *Sci Robot* **2019**, *4*.
[7] L. Wang, Y. Liu, Y. Cheng, X. Cui, H. Lian, Y. Liang, F. Chen, H. Wang, W. Guo, H. Li, M. Zhu, H. L. Ihara Wang, Y. Liu, Y. Cheng, X. Cui, H. Lian, Y. Liang, F. Chen, H. Wang, W. Guo Beijing Key, L. Wang, H. Li, M. Zhu, *Advanced Science* **2015**, *2*, 1500084.
[8] B. Wu, Y. Xue, I. Ali, H. Lu, Y. Yang, X. Yang, W. Lu, Y. Zheng, T. Chen, *Research* **2022**, *2022*.
[9] A. López-Díaz, A. Martín-Pacheco, A. M. Rodríguez, M. A. Herrero, A. S. Vázquez, E. Vázquez, *Adv Funct Mater* **2020**, *30*, 2004417.
[10] C. A. Aubin, S. Choudhury, R. Jerch, L. A. Archer, J. H. Pikul, R. F. Shepherd, *Nature 2019 571:7763* **2019**, *571*, 51.
[11] B. Mosadegh, P. Polygerinos, C. Keplinger, S. Wennstedt, R. F. Shepherd, U. Gupta, J. Shim, K. Bertoldi, C. J. Walsh, G. M. Whitesides, *Adv Funct Mater* **2014**, *24*, 2163.
[12] T. Spratte, C. Arndt, I. Wacker, M. Hauck, R. Adelung, R. R. Schröder, F. Schütt, C. Selhuber-Unkel, *Advanced Intelligent Systems* **2022**, *4*, 2100081.
[13] Y. Wang, R. K. Kankala, C. Ou, A. Chen, Z. Yang, *Bioact Mater* **2022**, *9*, 198.
[14] M. A. Skylar-Scott, S. G. M. Uzel, L. L. Nam, J. H. Ahrens, R. L. Truby, S. Damaraju, J. A. Lewis, *Sci Adv* **2019**, *5*.
[15] R. Niu, Y. Ding, L. Hao, J. Ren, J. Gong, J. Qu, *ACS Appl Mater Interfaces* **2022**, *14*, 45533.
[16] Q. Liang, F. Gao, Z. Zeng, J. Yang, M. Wu, C. Gao, D. Cheng, H. Pan, W. Liu, C. Ruan, Q. Liang, Z. Zeng, J. Yang, M. Wu, C. Gao, D. Cheng, H. Pan, C. Ruan, F. Gao, W. Liu, *Adv Funct Mater* **2020**, *30*, 2001485.
[17] G. Gao, J. H. Lee, J. Jang, D. H. Lee, J. S. Kong, B. S. Kim, Y. J. Choi, W. B. Jang, Y. J. Hong, S. M. Kwon, D. W. Cho, *Adv Funct Mater* **2017**, *27*, 1700798.
[18] L. Shao, Q. Gao, C. Xie, J. Fu, M. Xiang, Y. He, L. Shao, Q. Gao, C. Xie, J. Fu, Y. He, M. Xiang, *Adv Healthc Mater* **2019**, *8*, 1900014.
[19] X. Wang, X. Li, X. Dai, X. Zhang, J. Zhang, T. Xu, Q. Lan, *Colloids Surf B Biointerfaces* **2018**, *171*, 291.
[20] D. Wang, S. Maharjan, X. Kuang, Z. Wang, L. S. Mille, M. Tao, P. Yu, X. Cao, L. Lian, L. Lv, J. J. He, G. Tang, H. Yuk, C. K. Ozaki, X. Zhao, Y. S. Zhang, *Sci Adv* **2022**, *8*, 6900.
[21] M. Costantini, J. Idaszek, K. Szöke, J. Jaroszewicz, M. Dentini, A. Barbetta, J. E. Brinchmann, W. Święszkowski, *Biofabrication* **2016**, *8*, 035002.
[22] F. Shahabipour, M. Tavafoghi, G. E. Aninwene, S. Bonakdar, R. K. Oskuee, M. A. Shokrgozar, T. Potyondy, F. Alambeigi, S. Ahadian, *J Biomed Mater Res A* **2022**, *110*, 1077.
[23] X. Wang, Y. Yu, C. Yang, C. Shao, K. Shi, L. Shang, F. Ye, Y. Zhao, *Adv Funct Mater* **2021**, *31*, 2105190.
[24] X. Dai, L. Liu, J. Ouyang, X. Li, X. Zhang, Q. Lan, T. Xu, *Scientific Reports 2017 7:1* **2017**, *7*, 1.
[25] A. Kjar, B. McFarland, K. Mecham, N. Harward, Y. Huang, *Bioact Mater* **2021**, *6*, 460.
[26] R. Xie, Z. Liang, Y. Ai, W. Zheng, J. Xiong, P. Xu, Y. Liu, M. Ding, J. Gao, J. Wang, Q. Liang, *Nat Protoc* **2021**, *16*, 937.
[27] L. Andrique, G. Recher, K. Alessandri, N. Pujol, M. Feyeux, P. Bon, L. Cognet, P. Nassoy, A. Bikfalvi, *Sci Adv* **2019**, *5*, 6562.
[28] N. K. Singh, W. Han, S. A. Nam, J. W. Kim, J. Y. Kim, Y. K. Kim, D. W. Cho, *Biomaterials* **2020**, *232*, 119734.
[29] L. Shao, Q. Gao, C. Xie, J. Fu, M. Xiang, Y. He, *Biofabrication* **2020**, *12*, 035014.

[30] N. K. Singh, W. Han, S. A. Nam, J. W. Kim, J. Y. Kim, Y. K. Kim, D. W. Cho, *Biomaterials* **2020**, *232*, 119734.
[31] F. Tsegay, M. Elsherif, H. Butt, *Polymers 2022, Vol. 14, Page 1012* **2022**, *14*, 1012.
[32] L. K. Rivera-Tarazona, T. Shukla, K. A. Singh, A. K. Gaharwar, Z. T. Campbell, T. H. Ware, *Adv Funct Mater* **2022**, *32*, 2106843.
[33] A. Chen, W. Wang, Z. Mao, Y. He, S. Chen, G. Liu, J. Su, P. Feng, Y. Shi, C. Yan, J. Lu, *Advanced Materials* **2023**, 2307686.
[34] X. Wang, Y. Yu, C. Yang, C. Shao, K. Shi, L. Shang, F. Ye, Y. Zhao, *Adv Funct Mater* **2021**, *31*, 2105190.
[35] A. Sydney Gladman, E. A. Matsumoto, R. G. Nuzzo, L. Mahadevan, J. A. Lewis, *Nat Mater* **2016**, *15*, 413.
[36] D. Podstawczyk, M. Nizioł, P. Szymczyk-Ziółkowska, M. Fiedot-Toboła, *Adv Funct Mater* **2021**, 2009664.
[37] J. Simińska-Stanny, M. Nizioł, P. Szymczyk-Ziółkowska, M. Brożyna, A. Junka, A. Shavandi, D. Podstawczyk, *Addit Manuf* **2022**, *49*, 102506.
[38] H. M. Pan, A. Goto, *Macromol Rapid Commun* **2023**, *44*, 2300074.
[39] Y. Wang, H. Cui, T. Esworthy, D. Mei, Y. Wang, L. G. Zhang, *Advanced Materials* **2022**, *34*, 2109198.
[40] S. B. Gugulothu, K. Chatterjee, *ACS Macro Lett* **2023**, *12*, 494.
[41] L. Zeenat, A. Zolfagharian, Y. Sriya, S. Sasikumar, M. Bodaghi, F. Pati, *Adv Mater Technol* **2023**, 2300200.
[42] S. Miao, N. Castro, M. Nowicki, L. Xia, H. Cui, X. Zhou, W. Zhu, S. jun Lee, K. Sarkar, G. Vozzi, Y. Tabata, J. Fisher, L. G. Zhang, *Materials Today* **2017**, *20*, 577.
[43] J. Zhang, S. Yun, A. Karami, B. Jing, A. Zannettino, Y. Du, H. Zhang, *Bioprinting* **2020**, *19*, e00089.
[44] H. Li, Y. J. Tan, R. Kiran, S. B. Tor, K. Zhou, *Addit Manuf* **2021**, *37*, 101640.
[45] D. Maity, A. P. Teixeira, M. Fussenegger, *Small* **2023**, 2301427.
[46] C. O'Connor, E. Brady, Y. Zheng, E. Moore, K. R. Stevens, *Nature Reviews Materials 2022 7:9* **2022**, *7*, 702.
[47] K. Zhu, S. R. Shin, T. van Kempen, Y. C. Li, V. Ponraj, A. Nasajpour, S. Mandla, N. Hu, X. Liu, J. Leijten, Y. D. Lin, M. A. Hussain, Y. S. Zhang, A. Tamayol, A. Khademhosseini, *Adv Funct Mater* **2017**, *27*, 1605352.
[48] C. Colosi, S. R. Shin, V. Manoharan, S. Massa, M. Costantini, A. Barbetta, M. R. Dokmeci, M. Dentini, A. Khademhosseini, *Advanced Materials* **2016**, *28*, 677.
[49] M. Ilami, H. Bagheri, R. Ahmed, E. O. Skowronek, H. Marvi, *Advanced Materials* **2021**, *33*, 2003139.
[50] Y. Zhan, W. Fu, Y. Xing, X. Ma, C. Chen, *Materials Science and Engineering: C* **2021**, *127*, 112208.
[51] R. Singh, S. A. Deshmukh, G. Kamath, S. K. R. S. Sankaranarayanan, G. Balasubramanian, *Comput Mater Sci* **2017**, *126*, 191.
[52] E. Díez-Peña, I. Quijada-Garrido, J. M. Barrales-Rienda, *Macromolecules* **2002**, *35*, 8882.
[53] K. Cui, C. Yu, Y. N. Ye, X. Li, J. P. Gong, *Proc Natl Acad Sci U S A* **2022**, *119*, e2207422119.
[54] J. Jelken, S. H. Jung, N. Lomadze, Y. D. Gordievskaya, E. Y. Kramarenko, A. Pich, S. Santer, *Adv Funct Mater* **2022**, *32*.
[55] K. Sano, Y. Ishida, T. Aida, *Angewandte Chemie International Edition* **2018**, *57*, 2532.
[56] E. Appel, L. Heepe, C. P. Lin, S. N. Gorb, *J Anat* **2015**, *227*, 561.
[57] Y. Zhou, C. M. Duque, C. D. Santangelo, R. C. Hayward, Y. Zhou, R. C. Hayward, C. M. Duque, C. D. Santangelo, *Adv Funct Mater* **2019**, *29*, 1905273.
[58] S. Liu, E. Boatti, K. Bertoldi, R. Kramer-Bottiglio, *Extreme Mech Lett* **2018**, *21*, 35.

[59] Y. Zhang, P. Li, J. Quan, L. Li, G. Zhang, D. Zhou, *Advanced Intelligent Systems* **2023**, *5*, 2200071.
[60] K. Liu, Y. Zhang, H. Cao, H. Liu, Y. Geng, W. Yuan, J. Zhou, Z. Liang Wu, G. Shan, Y. Bao, Q. Zhao, T. Xie, P. Pan, K. Liu, Y. Zhang, H. Cao, H. Liu, Y. Geng, W. Yuan, J. Zhou, G. Shan, Y. Bao, Q. Zhao, T. Xie, P. Pan, Z. L. Wu, *Advanced Materials* **2020**, *32*, 2001693.
[61] H. Yuk, S. Lin, C. Ma, M. Takaffoli, N. X. Fang, X. Zhao, *Nat Commun* **2017**, *8*.
[62] X. Le, W. Lu, J. Zhang, T. Chen, *Advanced Science* **2019**, *6*, 1801584.
[63] Z. Chen, Y. Chen, C. Chen, X. Zheng, H. Li, H. Liu, *Chemical Engineering Journal* **2021**, *424*, 130562.
[64] T. Benselfelt, P. Rothemund, P. S. Lee, *Advanced Materials* **2023**, *35*.
[65] A. B. Baker, D. F. Wass, R. S. Trask, *Sens Actuators B Chem* **2018**, *254*, 519.
[66] C. Gilbert, T. Ellis, *ACS Synth Biol* **2019**, *8*, 1.
[67] I. Letnik, R. Avrahami, J. S. Rokem, A. Greiner, E. Zussman, C. Greenblatt, *Biomacromolecules* **2015**, *16*, 3322.
[68] A. Rodrigo-Navarro, S. Sankaran, M. J. Dalby, A. del Campo, M. Salmeron-Sanchez, *Nature Reviews Materials 2021 6:12* **2021**, *6*, 1175.
[69] T. Takahashi, *Molecules 2019, Vol. 24, Page 4441* **2019**, *24*, 4441.
[70] T. Christiani, K. Mys, K. Dyer, J. Kadlowec, C. Iftode, A. J. Vernengo, *JOR Spine* **2021**, *4*, e1161.
[71] X. Lin, X. Guan, Y. Wu, S. Zhuang, Y. Wu, L. Du, J. Zhao, J. Rong, J. Zhao, M. Tu, *Materials Science and Engineering: C* **2020**, *115*, 111123.
[72] Y. J. Chen, S. C. Wu, H. C. Wang, T. H. Wu, S. S. F. Yuan, T. Te Lu, W. F. Liaw, Y. M. Wang, *Mol Pharm* **2019**, *16*, 4241.
[73] A. Choi, K. D. Seo, H. Yoon, S. J. Han, D. S. Kim, *Biomater Sci* **2019**, *7*, 2277.
[74] R. Randriantsilefisoa, Y. Hou, Y. Pan, J. Luis Cuellar Camacho, M. W. Kulka, J. Zhang, R. Haag, R. Randriantsilefisoa, Y. Hou, Y. Pan, J. L. C Camacho, M. W. Kulka, J. Zhang, R. Haag, *Adv Funct Mater* **2020**, *30*, 1905200.
[75] S. Li, W. Wang, W. Li, M. Xie, C. Deng, X. Sun, C. Wang, Y. Liu, G. Shi, Y. Xu, X. Ma, J. Wang, *Adv Funct Mater* **2021**, *31*, 2102685.

Herein, inspired by a vascular system, a temperature-sensitive hydrogel with a network of permeable channels is fabricated by coaxial 4D printing. The thermoresponsivity of the hydrogel allows for temperature-dependent shape changes at both micro- and macro-scales. The macrostructure undergoes reversible shape transformation when transferred from cold to hot water and *vice versa*. At the microscale, the lumen diameter of the channels is controlled by temperature.

Daria Podstawczyk*, Piotr Śledzik, Martyna Nizioł, Julia Simińska-Stanny, Anna Dawiec-Liśniewska, Amin Shavandi

Coaxial 4D printing of vein-inspired thermoresponsive channel hydrogel actuators

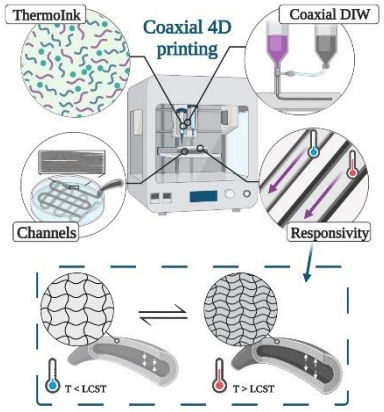

Supporting Information

Coaxial 4D printing of vein-inspired thermoresponsive channel hydrogel actuators

Daria Podstawczyk, Piotr Śledzik, Martyna Nizioł, Julia Simińska-Stanny, Anna Dawiec-Liśniewska, Amin Shavandi*

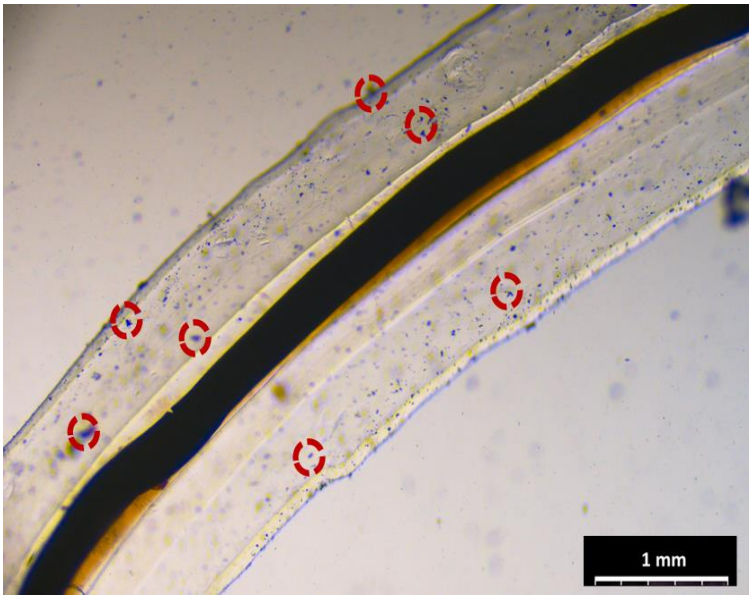

Figure S1. The optical image of the core-shell tubular construct shows that the core made of the sacrificial ink is being dissolved. Some examples of small fragments of the PF-127 outside the hydrogel are marked in red.

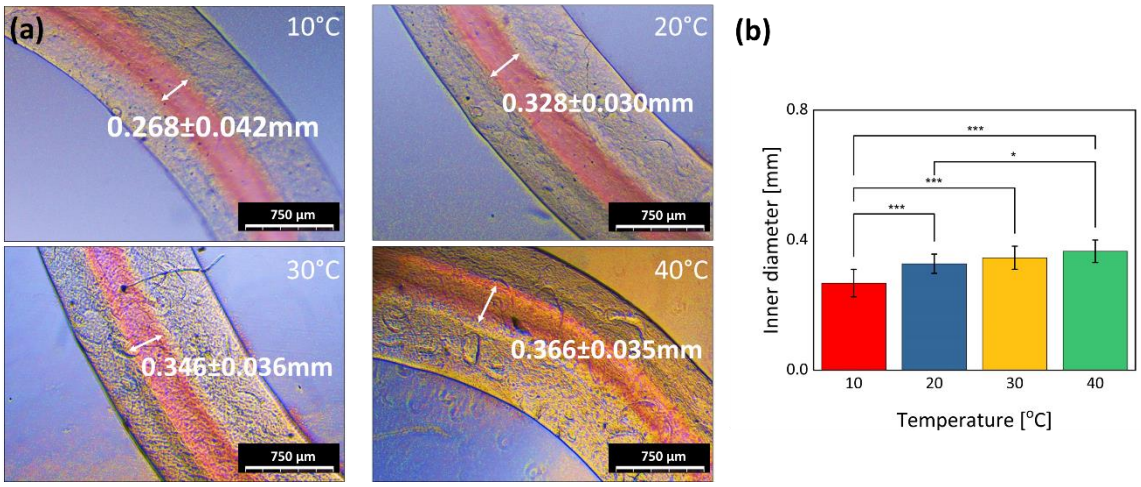

Figure S2. Stability of the printouts: (a) The optical images of the tubes 4 months post-printing; (b) Tube inner diameter as a function of temperature in the range of 10-40°C (n = 10)

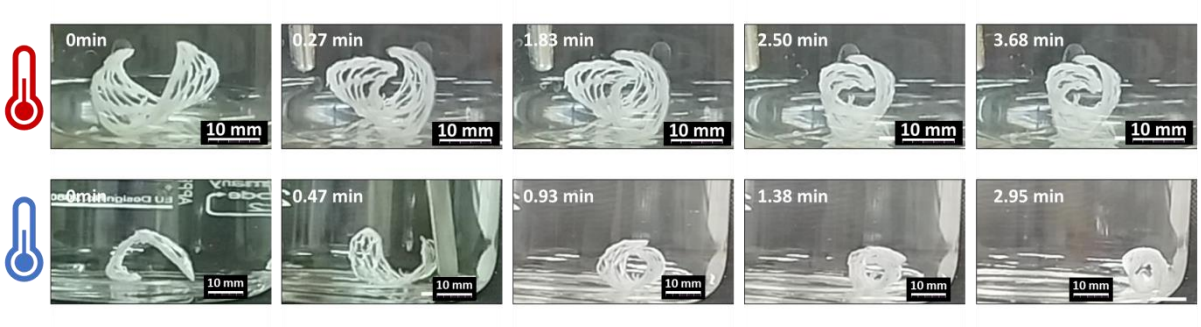

Figure S3. Reversible shape-morphing behavior of the channel hydrogel sheet (2LA) driven by temperature change.

Movie S1. Actuation of the channel scaffold in hot water. Upon immersion in water at 40°C, the scaffold undergoes shape deformation and unfolds.

Movie S2. Actuation of the channel scaffold in cold water. Upon immersion in water at 12°C, the scaffold undergoes shape deformation and rolls up.

Movie S3. Perfusion of the microalgae-containing medium in the hydrogel microtube. It includes the following steps: (1) the solution is injected into the tube lumen, and (2) microalgae diffuse longitudinally along the tube and reach the outlet.

Movie S4. Perfusion of the microalgae-containing medium in the channel network within the 4D-printed hydrogel. After the injection, the microalgae-containing medium immediately fills the interconnected channels demonstrating that the scaffold is permeable.